IEEE Access
Multidisciplinary ⋮ Rapid Review ⋮ Open Access Journal

Received March 30, 2021, accepted May 1, 2021, date of publication May 5, 2021, date of current version May 14, 2021.

Digital Object Identifier 10.1109/ACCESS.2021.3077649

Motion Characteristics of Metal Powder Particles in AC GIL and Its Trap Design

ZHENYU ZHAN[1,2], DONG WANG[1], (Member, IEEE), JUN XIE[3], WEIFENG XIN[1], WEI WANG[1], AND ZHENQIAN ZHANG[2]

[1]State Grid Henan Electric Power Research Institute, State Grid Henan Electric Power Company, Zhengzhou 450000, China
[2]China Electric Power Research Institute, Beijing 100192, China
[3]Hebei Provincial Key Laboratory of Power Transmission Equipment Security Defense, North China Electric Power University, Baoding 071003, China

Corresponding author: Zhenyu Zhan (zhanzhy_ha.sgcc@foxmail.com)

This work was supported by Science and Technology Project of State Grid Company Ltd., (Insulation Test Research and Engineering Application of UHV Converter Station GIS Equipment under Disturbance Condition) under Grant SGZB0000TGJS1901332.

ABSTRACT In view of the threat of metal particles to the insulation performance of AC GIL (Gas insulated transmission line), this paper uses aluminum powder to simulate the metal particles which are closer to the engineering practice, A scaled-down model similar to the actual GIL structure was built to study the movement characteristics of aluminum powder in GIL. The discharge, movement and distribution characteristics of aluminum powder was recorded in experiment. The research shows that the particles from spacer to the part below the shielding should be prevented. The particles with particle size of about 150 mesh move more violently. At the same time, the movement of powder particle in GIL is affected by Van der Waals force. According to the characteristics of particle motion distribution, grid-shaped trap and strip-shaped trap were designed and compared in this paper, and the trap capture coefficient was proposed. Finally, the suggestion of particle trap arrangement is put forward, that is, grid-shaped trap can be set near the spacer, and strip-shaped trap can be selected for the rest of the GIL.

INDEX TERMS AC GIL, aluminum powder, capture coefficient, particle trap, Van der Waals force.

I. INTRODUCTION

Due to the gas-insulated transmission line (GIL) has advantages such as low transmission losses, low capacitive load, large transmission capacity, high reliability, and suitable for long-distance power transmission, since the 1970s, Germany, U.S., Japan, and other countries have been established 72∼1200 kV GIL successively. At present, the global GIL installation length has exceeded 700 km. With the development of technology, GIL is gradually replacing traditional electric cables and overhead transmission lines, becoming the trend of power transmission in the future [1], [2].

In recent years, GIL has been developing towards a higher voltage level and installing in a more complex environment. However, during the production, transportation, and installation of GIL, due to the influence of welding, abrade of sliding spacers and construction environment, powder and other particles will be inevitably introduced in the cavity.

These particles are charged and forced to move in the nonuniform electric field in the GIL, which is easy to adsorb on the spacer surface, causing the distortion of the surrounding electric field, resulting in the breakdown of the gas gap or spacer, which is very easy to cause GIL insulation failure [3], [4]. Relevant research has shown that the existence of metal particles could reduce the insulation strength of GIL/GIS by more than 90%. According to the statistics of the International Conference on Large High Voltage Electric System (CIGRE), the insulation fault caused by metal particles and foreign objects has exceeded 20%, which has become the major factor affecting the stable operation of the gas insulated equipment [5], [6].

Scholars from the Britain, Japan and other countries have used ultra-high frequency (UHF) and other methods to monitor partial discharge caused by particles in the GIL. The results show that the UHF method has good detection performance in both laboratory and the practical. According to the collected discharge signals, the position of the particles can be calculated more accurately. At the same time, it was also found that the moving particle produces a much larger partial discharge signal than the stationary particle [7]–[9]. Reference [10] studied the discharge characteristics of metal particles under different voltage waveforms, and proposed a

The associate editor coordinating the review of this manuscript and approving it for publication was Junjian Qi.

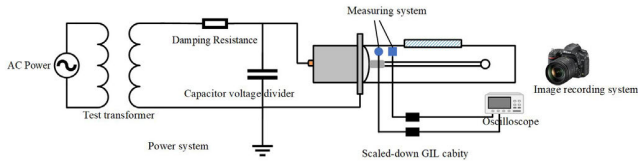

FIGURE 1. The scaled-down GIL particle motion experiment platform.

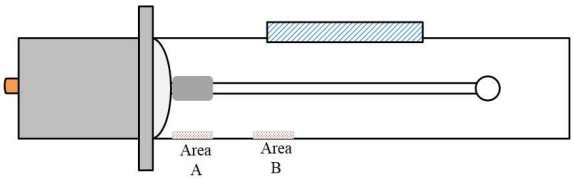

FIGURE 2. Schematic diagram of particle placement area.

method to characterize the severity of particle discharge by analyzing the statistical spectra. Some scholars have found that the ultrasonic signal of the particle movement in the AC GIL has some randomness, the phase correlation with the applied voltage is weak, and the particle flight time increases with applied voltage increase [11], [12]. Reference [13] used the pulse current method and the ultrasonic signal to reckon the size of the line shape particles in the GIL.

In order to reveal the harm of particles to GIL, the research of particles in GIL has gradually changed from the discharge characteristics to the movement of particles. Sakai obtained the forced and charged equation of particle in plate electrodes [14]. [15]. Jia Jiangbo analyzed the spherical and linear particles in the wedge-shaped electrode under AC conditions and found that the existence of spacer would reduce the lifting voltage of the particles and also make the particle move towards the spacer [16]. Li Qingmin improved the force calculation of spherical and line shape particles under DC, and the coaxial cylindrical electrode was used to verify the validity of the model [17], [18]. To ensure the safe and stable operation of GIL manufacturers and research institutions have proposed to use particle trap, conductor coating and embedded electrode to improve the lifting voltage of metal particles [19], [20].

The charged and forced conditions of particles becomes complicated with the continuous changes of the applied voltage under AC conditions, there are few studies on the motion characteristics of particles in the AC GIL at present. In addition, in order to simplify the analysis, most of the researches focus on single spherical or line shape particle, which often ignore the influence of powder particle. The GIL field assembly process has strict specifications requirements so it is difficult for large particles to remain in GIL. The threat of powder particles to GIL insulation cannot be ignored [21], [22].

In this paper, a scaled-down experiment platform with the same structure as the full-scale AC GIL was established, different size powder metal particles were used to simulate the actual particles in the GIL, and the distribution characteristics of the powder under the rated voltage are calculated. Based on the particle distribution characteristics, traps of different shapes were set to capture particles, and their capturing ability was evaluated, and trap setup suggestions in AC GIL were put forward.

II. GUIDELINES FOR MANUSCRIPT PREPARATION

A. EXPERIMENT PLATFORM

The scaled-down GIL experiment platform designed in this paper is shown in Fig. 1. The platform is mainly include power system, scaled-down GIL cavity, measuring system and image recording system. The power system is composed of NRIGTB-5/50 AC test transformer and NRIRCF-50kV capacitor voltage divider, which mainly provides AC power for the experiment cavity. The structure of the scaled-down experiment cavity is modeled on the full scale 126 kV GIL, including spacers, shield and other structures, the cavity size is 1/2 of the full-scale cavity. The rated phase voltage of the cavity is 31.5 kV according to the ratio calculation. The inner diameter of the scaled-down cavity is 125 mm, and the total length of the cavity is 105 cm. The experiment is carried out in the longest section (length:70 cm) of the cavity with a 20 cm $\times$ 10 cm observation window on the side, which is used to set the light and observe the movement of particles inside the cavity. The other end of the cavity is plexiglass, which is applied for recording the motion characteristics of particles. The measuring system consists of ultrasonic sensor and UHF sensor which is used to record the vibration signal generated by the collision of particles with the cavity and the partial discharge signal that may occur inside the cavity. The ultrasonic sensor is R3α with a 40 kHz resonance frequency. The UHF sensor is ZKA-1, the ultrasonic signal is amplified by a 60 db amplifier, and the UHF sensor is detected by the detection module and then connected to the Tektronix DPO2024B oscilloscope for signal acquisition. The image recording system mainly uses Nikon D750 camera to record particles movement.

B. EXPERIMENT SCHEME

GIL cavity is mainly made of aluminum and other metal materials. By statistical analysis of the main elements of solid particles collected in GIL during operation, it was found that the solid particles in GIL mainly contain Al, Cu, Fe and other metal elements. For this reason, 50 mesh, 150 mesh, and 250 mesh aluminum powder selected to simulate metal particles that may appear in the GIL in the experiment.

The relationship between the mesh and the particle size is shown in Table.1. Before each experiment, the inner wall of the cavity should be wiped by alcohol to avoid charge accumulation, after that, weigh 1 g of the same size particles, and use a rectangular groove to send the particles into a designated area as shown in Fig. 2, then spread the particles evenly with area of 5 cm $\times$ 1 cm. Area A corresponds to the position directly below the shield, which is 5$\sim$10 cm away from the spacer, and area B corresponds to the position bellow the rod, which is 15-20 cm away from the spacer.

After placed the particles in the specified area, the cavity was pumped into the vacuum state slowly and uniformly,

TABLE 1. Mesh and diameter conversion.

Mesh	50	150	250
Particle Diameter/μm	270	106	58

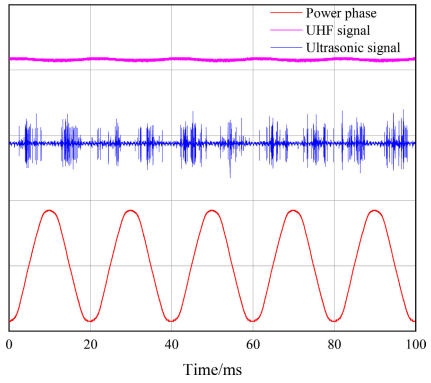

FIGURE 3. Typical signal during particle motion.

TABLE 2. Powder particle lifting voltage.

Initial Area \ Mesh	50	150	250
A	24 kV	14 kV	28 kV
B	26 kV*	24 kV	30 kV*

*When the initial area of 50 mesh and 250 mesh aluminum powder was in area B, only a few particles were observed lifting-off.

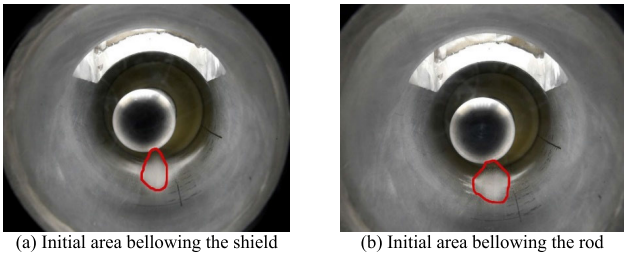

(a) Initial area bellowing the shield (b) Initial area bellowing the rod

FIGURE 4. Motion image of 150 mesh aluminum powder at different initial position.

then the experiment cavity was filled with 0.2 MP SF_6. The voltage of the cavity was raised to the rated value at the speed of 0.1 kV / s by increasing the voltage evenly, and the rated voltage was maintained for 5 min. The ultrasonic and UHF signals were recorded, and the gas in the chamber was slowly released after the voltage was reduced. By using the analytical balance, ratio of mass distribution in the cavity of different powder was calculated at every centimeter.

III. EXPERIMENT RESULTS

Fig. 3 shows the typical UHF and ultrasonic signals collected in an experiment. Haar wavelet is used to denoise the collected signals [23]. From the figure that the UHF signal is weak, no obvious pulse signal is found, and the ultrasonic sensor can collect obvious signal. For the particles with smaller size, the micro discharge is weak, and the ultrasonic signal can be considered as the vibration signal produced by the collision between the particles or with the experiment cavity [20]. In order to avoid the error caused by the experiment, each group of experiments was carried out many times. Because the particle distribution characteristics of each group of experiments are basically similar, one group of them was taken as a typical experiment result for analysis.

A. MOTION CHARACTERISTICS OF METAL POWDER WITHOUT TRAPS

After applied voltage, the motion characteristics of aluminum powder with different mesh number at different initial area were also different. The powder particle lifting voltage is shown in Table.2. And there is no linear relationship between the lifting voltage and the mesh number of particles. When the particle mesh number reaches 150 mesh, the particles have the lowest lifting voltage. Since the electric field intensity at the cavity shield (area A) is relatively concentrated, therefore, when the mesh number is the same, the lifting voltage of the particles under the shield is lower than that below the rod.

Fig.4 shows the image of the initial position of 150 mesh aluminum powder bellowing the shield or rod During applying the voltage, the particles under the shield moving more obviously. Through the observation window of the upper cavity, the particles repeatedly and irregularly jump in the cavity gap. Most of the particles gradually moved away from the spacer, and some of them moved towards the spacer. The particles moved irregularly in the radial direction as well as in the axial direction of the cavity, and gradually distributed on the surface of the inner wall of the cavity. As the particles were continuously dispersed, the moving particles were gradually reduced. When the initial position of the particles was bellowing the rod, most of the particles of 50 mesh and 250 mesh aluminum powder did not move obviously except a few of them moved towards the spacer. However, 150 mesh aluminum powders remained moving, and the moving mode was similar to that of the initial position under the shield.

When the voltage was increased to the rated voltage, the typical filtered ultrasonic signals of aluminum powder with different mesh is shown in Fig. 5. The ultrasonic signal shows strong randomness, the amplitude of the ultrasonic signal was larger near the zero-crossing point of the voltage. With the decreased of the size of particles, the amplitude of the ultrasonic signal decreased gradually. Considering the case of single particle, the correlation between ultrasonic signal and phase is weak, especially for the multiple powder particles. When the voltage is in the positive half cycle or negative half cycle of AC, the particle is subjected to a single direction of electric field force, the direction of acceleration remains unchanged, and the velocity of particle motion continues to increase. When the voltage decreases gradually close to the zero-crossing point, the velocity reaches the maximum value, and the particle colliding with the cavity

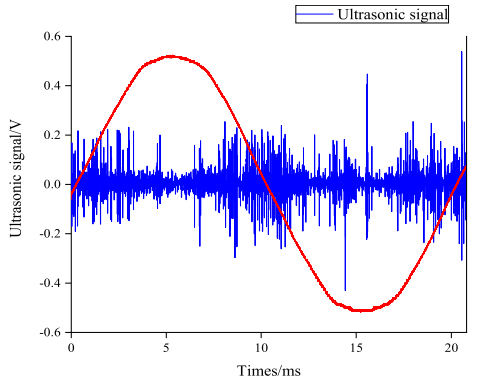

(a) 50 mesh aluminum powder initial in area A

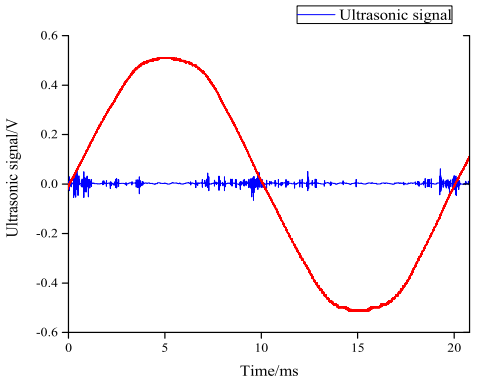

(b) 50 mesh aluminum powder initial in area A

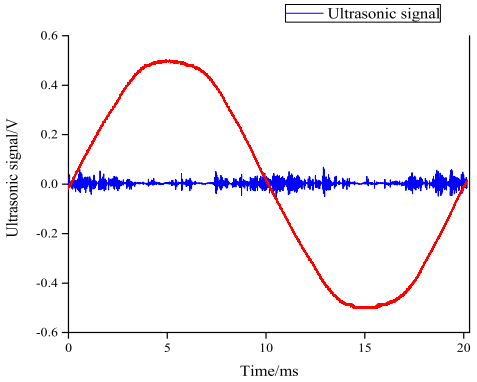

(c) 50 mesh aluminum powder initial in area A

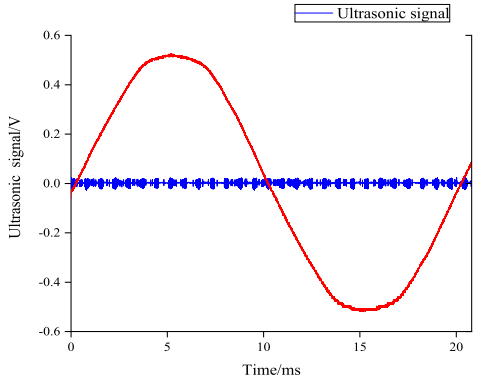

(d) 50 mesh aluminum powder initial in area A

FIGURE 5. Typical ultrasonic signal.

has a larger contact force, which makes the ultrasonic signal larger. However, when the mesh number increases, that is, the particle size decreases, the contact force produced by

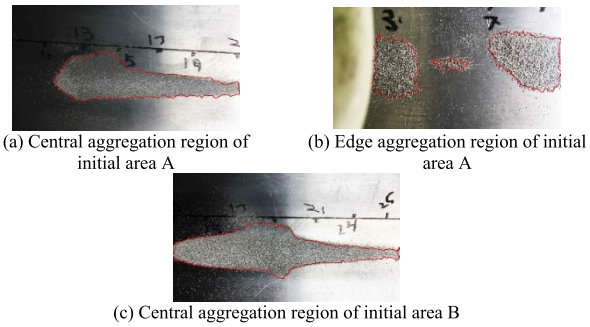
(a) Central aggregation region of initial area A

(b) Edge aggregation region of initial area A

(c) Central aggregation region of initial area B

FIGURE 6. Typical distribution of aluminum powder at different initial area.

the particle colliding with the cavity also decreases, so the amplitude of the ultrasonic signal also decreases [12].

The distribution of 150 mesh aluminum powder in different initial areas after applying voltage is shown in Fig.6. After the experiment, the particles were not completely dispersed inside the cavity, but were aggregated among several areas. No matter where the particles were initially placed, there will be a large area of central aggregation region under the rod, and there will be a small area of edge aggregation area near the spacer, and each area had a clear division between each other. When the initial position of the particles was in the area A, the central aggregation region of the particles after the experiment was similar to that of the water droplets, and the tail of the water droplets was towards the spacer side. When the initial position of the particles is in the area B, the central aggregation region of the particles was similar to a symmetrical spindle.

Fig. 7 shows the mass proportion distribution of aluminum powder with different mesh when the initial position was in area A, and the distribution of aluminum powder with 150 mesh at different initial positions. From Fig. 7(a) that most of the particles were gathered far away from the spacer after the voltage was applied, and a small part of the particles were still gathered near the spacer. Compared with the aluminum powder with different meshes, 150 mesh aluminum powder was widely distributed, and it was still distributed in clusters far away from the spacer. According to the distribution shown in Fig. 7(b), when the initial position of the aluminum powder was in area B (15 $\sim$ 20 cm away from the spacer), most of the aluminum powder was still located in area B after the experiment, and the mass of moving particles was less than that of the aluminum powder which initial position was in area A.

B. TRAP DESIGN AND EVALUATION

Since the electric field intensity under the shield is relatively concentrated, particles located below the shield are easy to lift-off, and particles often cause spacer surface flashover. Therefore, the area from the spacer to the area under the shield is the key protection area, and traps are needed in this area. In the experiment, it was found that most

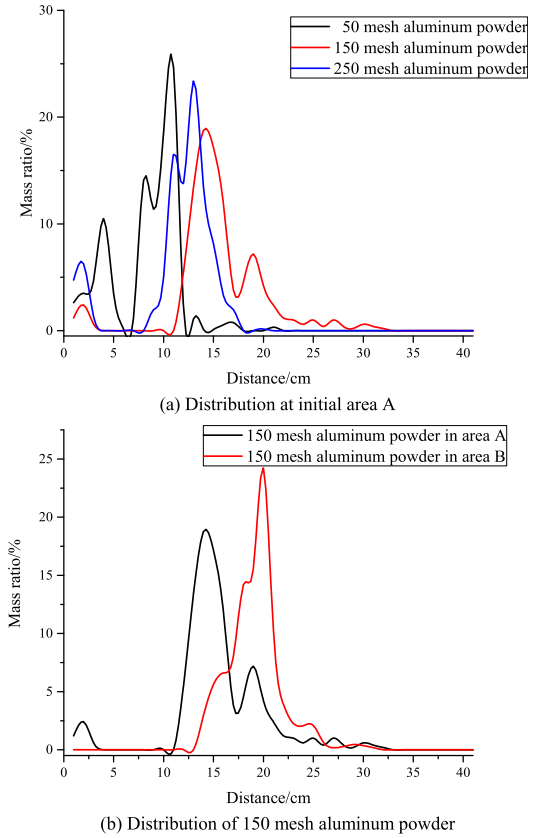

FIGURE 7. Particle distribution.

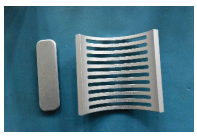

FIGURE 8. Image of particle trap.

of the powder particles move away from the spacer under AC condition, if conditions permit, particle traps should also be set below the rod to restrain particle movement. The trap position set in the experiment was located directly under the shield.

In this paper two types of traps were designed: grid-shaped and strip-shaped. The image of the trap is shown in Fig. 8. S. J. Dale's research shows that under AC conditions, most of the particles rolled in from the bottom of the trap, and a small part of the particles felled into the slot from the top of the trap [24]. Therefore, both traps have a 3mm gap between the traps and the inner wall of the cavity, so that the particles can roll into the trap. For grid-shaped trap, three parameters of trap should be controlled, thickness, slot width and slot spacing. Strip-shaped trap should control the thickness and width. The specific trap parameters and numbers are shown in Table. 3.

In order to avoid the electric field distortion caused by the trap itself and reduce the GIL insulation performance

TABLE 3. Particle trap parameter.

No.	Type	Slot Width×Slot Spacing/mm	Thickness/mm
A	Grid-shaped	5×5	5
B	Grid-shaped	5×5	3
C	Grid-shaped	5×8	5
D	Grid-shaped	8×5	5
No.	Type	Width/mm	Thickness/mm
E	Strip-shaped	30	5
F	Strip-shaped	30	3
G	Strip-shaped	25	5

after setting the trap. The finite element software was used to calculate the electric field distribution near the trap under the condition of peak AC voltage. The electric field distribution at the upper, middle, and lower parts of the trap is shown in Fig. 9. Since the trap length is longer than the shield, the electric field intensity distribution is not symmetrical. The calculation results show that the field strength near the trap is within the control value after the trap is set, which meets the GIL insulation design [2]. According to the calculation results of the electric field, the electric field in the grid-shaped trap is not a smooth curve due to the existence of the slot structure. The electric field in the slot is obviously concentrated, and the particles falling into it may escape; because of avoiding the slot structure, the electric field distribution of the strip-shaped trap is more uniform, especially at the lower part of the trap, the field strength is lower, which can effectively prevent the falling particles escaping from the trap by the electric field force

Experiment showed that the movement of 150 mesh aluminum powder is obvious. In this paper, 150 mesh aluminum powder was selected to test the trapping effect of different traps, to verify the effectiveness of particle traps. In the experiment, 1 g 150 mesh aluminum powder was weighed each time, and with the area of 5 cm × 1 cm was evenly spread under the trap or 2 cm in front of the trap. After applying voltage for 5 min, and the trapping effect was observed.

When the particles were directly below the trap, the grid-shaped trap and strip-shaped trap capture typical ultrasonic

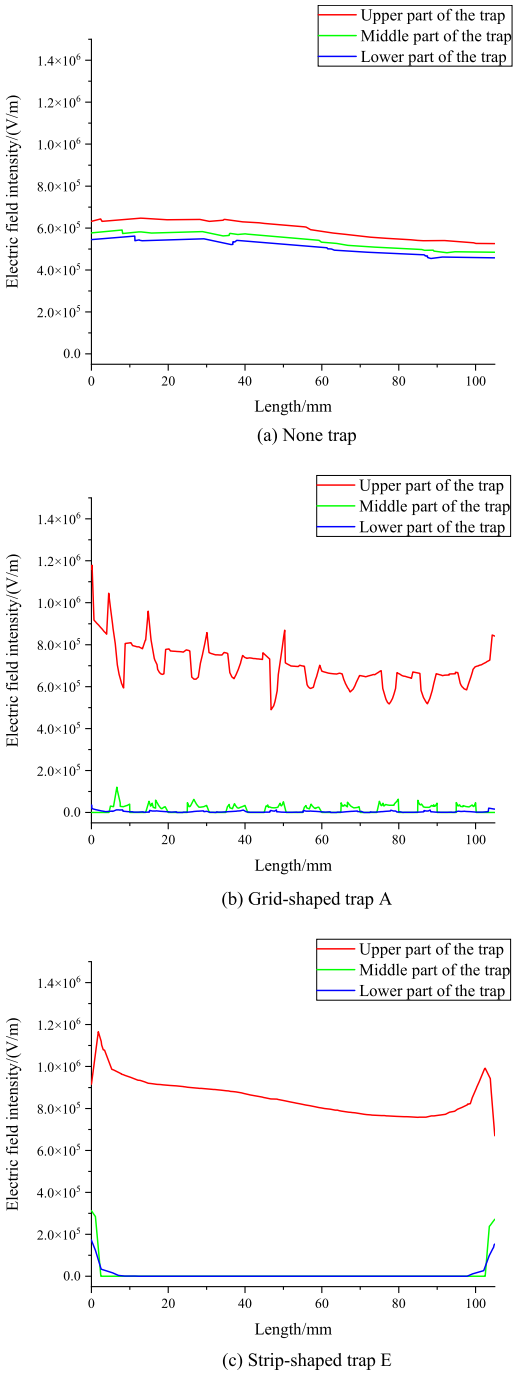

FIGURE 9. Electric field intensity near none trap or typical traps.

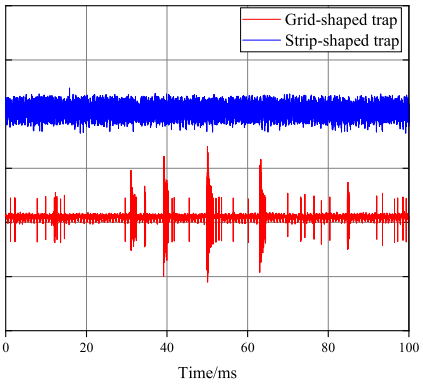

FIGURE 10. Ultrasonic signal of particles located below the particle trap.

signals, as shown in Fig. 10. When grid-shaped trap was used, strong ultrasonic signal will be detected, whereas the strip-shaped trap was used, weak ultrasonic signal will be detected. When the trap was removed after the experiment, the distribution of particles under the grid-shaped trap can be seen to change. Because the electric field of the corresponding part of the slot under the grid-shaped trap is still distorted, the particles trapped by the grid-shaped trap still have the possibility of lifting, while the electric field under the strip-shaped trap is very weak, once the particles were trapped by the strip-shaped trap, they will no longer be affected by the electric field force and will not move. In the experiment, no particles were found outside the grid-shaped trap or the strip-shaped trap.

When the particle position was in front of the trap, the typical signals collected under different trap settings are shown in Fig. 11. Fig. 11 (a) shows a group of typical signals when only trap was set and no particles were placed. UHF and ultrasonic signals were not detected when only traps were placed, which can prove that the traps designed in the experiment did not produce partial discharge or vibration signals. After placing the particles, both the grid-shaped trap and strip-shaped trap with thinner thickness can detect strong ultrasonic signals and UHF signals (Fig. 11 (c) and Fig. 11 (g)), and the particle motion was relatively high, especially in the thin grid-shaped trap. In other types of traps, the ultrasonic signal amplitude was relatively weak, and no partial discharge signal was collected, which shows that the thinner trap has a threat to the insulation.

When the grid-shaped trap was set, most of the particles fall on the first slot and the edge of the trap, which is similar to S. J. Dale's study [24]. When the strip-shaped trap was set, besides to the particles below the edge of the trap near the initial position of the particles, some particles also appeared on the side far away from the initial position of the particles.

Because the strip-shaped trap is narrow, it cannot cover the whole inner wall of the cavity. Besides the axial direction, the particles also moved randomly in the radial direction, so some particles will cross the trap. Whether it is grid-shaped trap or strip-shaped trap, in addition to the particles moving below and near the trap, a small number of particles move away from the trap after the experiment. After setting the trap,, particles are mainly divided into three states: capture, immobile and escape.

According to this, this paper proposes the trap capture coefficient F_{trap}, the equation is as follows

$$F_{trap} = \frac{M_{cap}}{M_{esc}} \times \left(\frac{1}{T_{PD}+1}\right)^2 \tag{1}$$

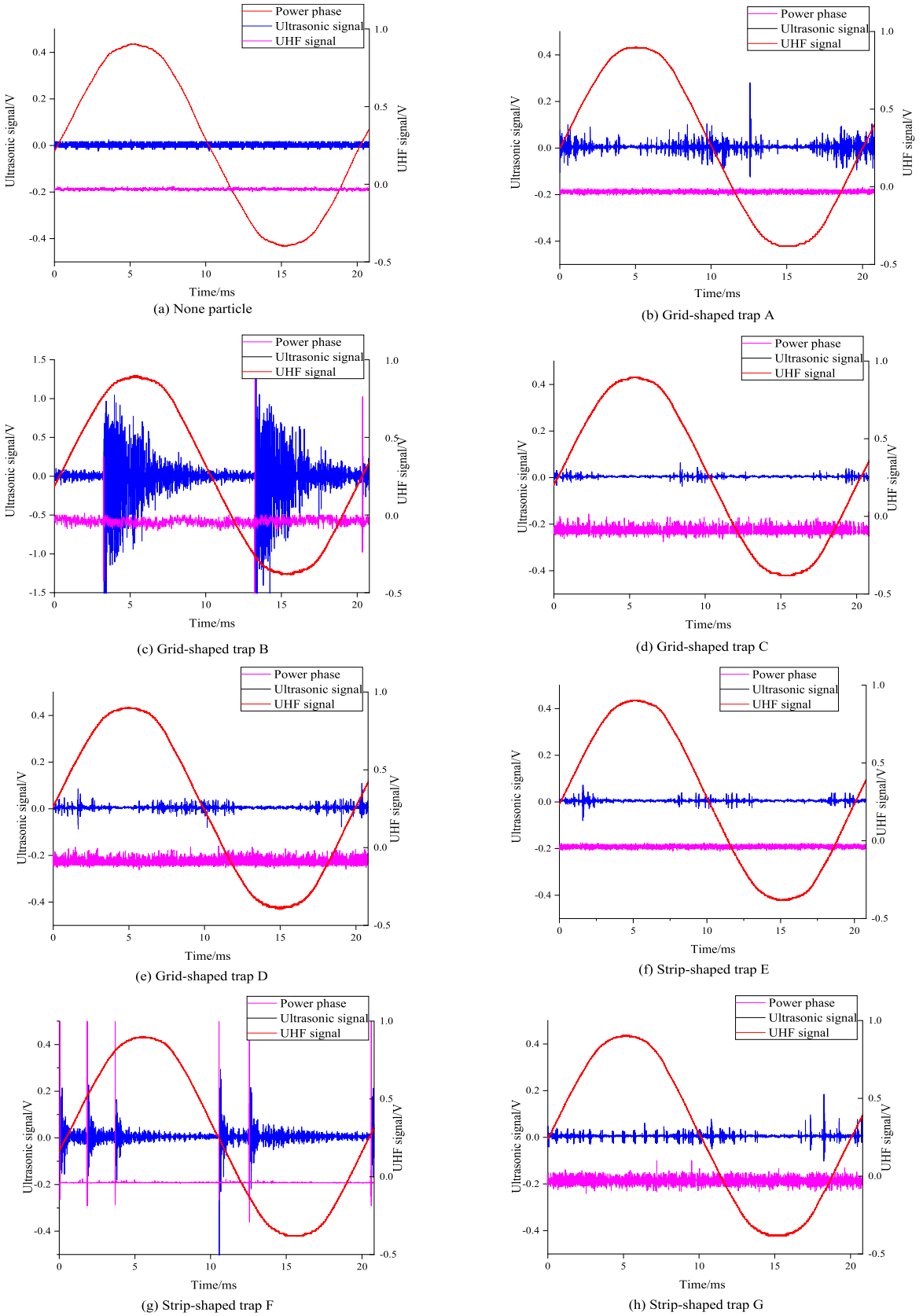

FIGURE 11. Typical signal under different particle trap.

TABLE 4. Particle trap parameter.

Type of Trap	Trap Coefficients
Grid-shaped A	0.66
Grid-shaped B	0.24
Grid-shaped C	3.16
Grid-shaped D	5.57
Strip-shaped E	0.79
Strip-shaped F	≈0 (Value too small)
Strip-shaped G	0.24

where, M_{cap} represents the mass of trapped particles, M_{esc} is the mass of escaped particles, and $_{\mathrm{TPD}}$ is the number of pulse partial discharge signals that is greater than 0.2 V in per AC frequency cycle, the larger the coefficient, the better the trap capturing effect. The trap coefficients of different traps are shown in Table. 4.

According to the experiment and analysis, under the condition that traps meet the electric field control value, traps with larger thickness should be set to reduce the micro discharge when trapping particles. For this example, the trap with 5 mm thickness is selected. By calculating the trapping coefficient, the trapping coefficient of grid-shaped trap is generally greater than that of strip-shaped trap because the escape of particles in grid-shaped trap is not obvious. The slot width of the grid-shaped trap has a great influence on the capture coefficient, and the grid-shaped trap with larger slot width has better capture effect and in this case, slot width choose 8 mm. For the strip-shaped trap, its capture coefficient is positively related to its width. Because the strip-shaped trap cannot cover the bottom of the cavity comprehensively, the particles may cross the trap from the side of the cavity, especially near the spacer, the trap is difficult to fit closely with the spacer and other partitions, which will cause the escape particles to gather in the area. The larger the width of the strip-shaped trap, the wider the coverage, which can reduce the particles. At the same time, the electric field under the strip-shaped trap is very weak, and there is no sudden change of electric field caused by the grid trap slot, so the strip trap can be installed bellow the rod.

Based on the above results and considering the welding manufacturing of the two type traps, it is considered that the grid-shaped traps with large slot width should be used in the key areas of the cavity, especially near the spacer, on the premise of meeting the requirements of the design electric field intensity. If the conditions are met, for key projects, a wide strip trap can be set under the rod to realize all-round protection of the cavity.

IV. DISCUSSION

At present, many researches have been carried out on the motion force of a single particle. It is generally believed that in the electric field, metal particle is mainly affected by the gravity, Coulomb force, electric field gradient force, gas resistance, and frictional force after being charged in an electric field. Fig.12 is a schematic diagram of the force on particles. The equation for calculating the force on particles are shown in (2) ∼ (7) [14], [25]–[27]:

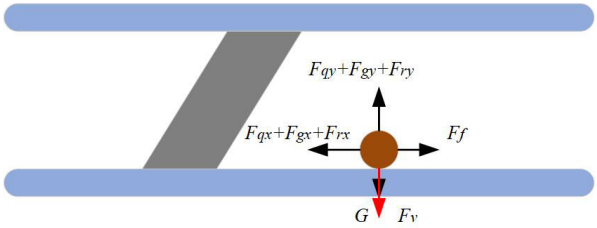

FIGURE 12. Schematic diagram of the force on particles.

Gravity (G):

$$G = mg = \frac{4}{3}\rho\pi r^3 g \tag{2}$$

where ρ is the density of the particles and r is the radius of the particles.

When the metal particles collide with the electrode plate, the charge amount and polarity of the particles in the electric field are determined by the electric field intensity E_0 of the position where the particles collide with the electrode plate last time and the polarity of the electrode, that is:

$$Q = \frac{2\pi^3}{3} r^2 \varepsilon_0 \varepsilon_s E_0 \tag{3}$$

where ε_0 is the dielectric constant in vacuum; ε_s is the relative dielectric constant of gas.

From this, calculate the Coulomb force Fq on particles in the electric field:

$$F_q = k_1 QE \tag{4}$$

where k_1 represents the electrostatic force correction coefficient. When the particles are in contact with the electrodes, $k_1 = 0.832$, when the particles are suspended between the electrodes, $k_1 = 1$. E is the electric field intensity at the position of the particle, and the electric field gradient force F_g applied to the charged particle is:

$$F_g = 2\pi r^2 \varepsilon_0 \varepsilon_s \left| \nabla E^2 \right| \tag{5}$$

The moving particles will be affected by the resistance in the gas. According to the Stokes resistance calculation formula, the gas resistance F_d of the particles is:

$$F_d = 6\pi\eta v \tag{6}$$

where η is the drag coefficient and v is the particle velocity.

Friction of moving particles:

$$F_f = \mu \left(G - F_{qy} - F_{gy} \right) \tag{7}$$

where μ is the rolling friction coefficient.

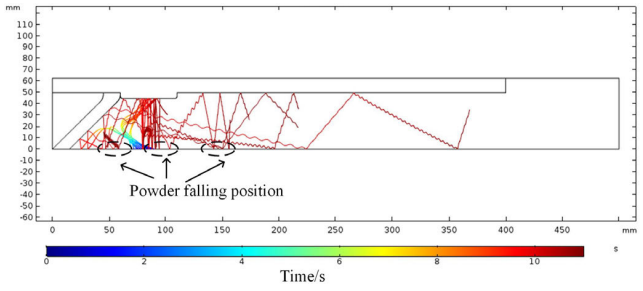

FIGURE 13. Particle motion simulation.

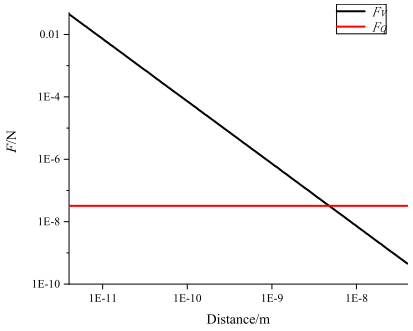

FIGURE 14. Comparison of Van der Waals force and Coulomb force.

The simulation model was established according to the experiment, and the motion characteristics of particles under AC condition were calculated by using the finite element method. Fig. 13 shows the motion results of multiple particles within 11 s.

The simulation results show that the motion characteristics of particles located in different positions of the cavity are complex, and there is no unified direction of motion. There are particles moving towards the spacer and also some moving away from the spacer. The particles are reciprocated in the cavity under the action of AC electric field, and the falling position have aggregation.

In the actual cavity, due to the roughness of the cavity surface [28], there is a certain randomness in the direction of particle lifting and rebound, and the particles after lifting are affected by the discharge ion wind between other particles, so the actual particle movement is more complex.

For powdery particles, it will be affected by Van der Waals force, which can be calculated by (8)

$$F_v = \frac{Ad}{12Z_0^2} \tag{8}$$

where A is the hamaker constant, the hamaker constant of aluminum is 1.5×10.19, d is the particle diameter, and Z_0 is the Van der Waals force range. The curve of electric force (Sum of Coulomb force and electric field gradient) and Van der Waals force of 250 mesh particles varying with the gap distance of particles is shown in Fig. 14. After aggregation of particles with different particle sizes, the distances between particles are different.

When the particle gap is too small, the Van der Waals force will be greater than the electric field force, resulting in the phenomenon that the particles do not lift [29],[30]. When the particles are lifted, the moving particles are also affected by the Van der Waals force, which makes the particles agglomerate. A small part of the particles moves towards the spacer, whereas most of the particles are far away from the spacer. As a result, the final distribution of the particles will appear larger central aggregation region and smaller edge aggregation region.

V. CONCLUSION

Experiments on the motion characteristics of metal particles in a scaled-down AC GIL model cavity were carried out. The experiments results show that the particle movement under the GIL shield is relatively strong, which should be the key protection area.

The distribution of particles under AC voltage were obtained. The central aggregation area of particles with initial position under the shield is similar to that of water droplets, and the central aggregation area of particles with initial position bellowing rod is similar to that of spindles. The effect of Van der Waals force should be considered for powder particles. The particle simulation model under AC condition is established

Grid-shaped traps and strip-shaped traps with different parameters were designed, and the trapping coefficient used to characterize the trapping effect is proposed. It is considered that, when the design permits, thicker traps should be used, grid traps with larger slot width should be set under the spacer to the shield, and strip-shaped traps with larger width should be set in the rest of the pipeline, which have better protection effect on metal and semiconductor particles;

REFERENCES

[1] H. Koch, *Gas Insulated Transmission Lines (GIL)*. Hoboken, NJ, USA: Wiley, 2012.

[2] P. Li, X. Yan, H. Wang, Q. Zhang, G. Jin, Y. Gao, and S. Mu, "Research and application of UHVAC gas-insulated transmission line," *Power Syst. Technol.*, vol. 41, no. 10, pp. 3161–3167, Oct. 2017.

[3] Q. Li, J. Wang, and B. Li, "Review on metal particle contamination in GIS/GIL," *High Voltage Eng.*, vol. 42, no. 3, pp. 849–860, Mar. 2016.

[4] H. Kuwahara, S. Inamura, T. Watanabe, and Y. Arahata, "Effect of solid impurities on breakdown in compressed SF6 gas," *IEEE Trans. Power App. Syst.*, vol. PAS-93, no. 5, pp. 1546–1555, Sep. 1974.

[5] A. H. Cookson, "Review of high-voltage gas breakdown and insulators in compressed gas," *IEE Proc. A, Phys. Sci., Meas. Instrum., Manage. Educ., Rev.*, vol. 128, no. 4, pp. 303–312, May 1981.

[6] *Insulation Coordination of GIS: Return of Experience, on Site Tests and Diagnostic Techniques*, CIGRE Joint Working Group, Paris, France, 1998.

[7] M. D. Judd, O. Farish, and B. F. Hampton, "The excitation of UHF signals by partial discharges in GIS," *IEEE Trans. Dielectr. Electr. Insul.*, vol. 3, no. 2, pp. 213–228, Apr. 1996.

[8] T. Hasegawa, K. Yamaji, M. Hatano, F. Endo, T. Rokunohe, and T. Yamagiwa, "Development of insulation structure and enhancement of insulation reliability of 500 kV DC GIS," *IEEE Trans. Power Del.*, vol. 12, no. 1, pp. 194–202, Jan. 1997.

[9] S. Okabe, T. Yamagiwa, and H. Okubo, "Detection of harmful metallic particles inside gas insulated switchgear using UHF sensor," *IEEE Trans. Dielectr. Electr. Insul.*, vol. 15, no. 3, pp. 701–709, Jun. 2008.

[10] H. Ji, C. Li, Z. Pang, B. Qi, and S. Zheng, "Influence of voltage waveforms on partial discharge characteristics of GIS mobilized metal particles," *Trans. China Electrotechnical Soc.*, vol. 31, no. 13, pp. 218–226, 2016.

[11] X. Y. Tan, H. Guo, Q. G. Zhang, and J. ZHANG, "DC ultrasonic characteristics and states recognition of motion metallic particles in GIS," *High Voltage Eng.*, vol. 36, no. 2, pp. 391–395, Feb. 2010.
[12] D. Li, J. Yang, J. Liang, and L. Wu, "Characteristics of acoustic signal from free moving metallic particles in gas insulated switchgear," *J. Xi'an Jiaotong Univ.*, vol. 43, no. 2, pp. 101–105, Feb. 2009.
[13] Z. Xizi, "Size estimation of linear metal particle based on the collision frequency and discharge amplitude," *High Voltage App.*, vol. 53, no. 4, pp. 107–115, Apr. 2017.
[14] K. Sakai, D. Labrado Abella, J. Suehiro, and M. Hara, "Charging and behavior of a spherically conducting particle on a dielectrically coated electrode in the presence of electrical gradient force in atmospheric air," *IEEE Trans. Dielectr. Electr. Insul.*, vol. 9, no. 4, pp. 577–588, Aug. 2002.
[15] K. Sakai, S. Tsuru, D. L. Abella, and M. Hara, "Conducting particle motion and particle-initiated breakdown in DC electric field between diverging conducting plates in atmospheric air," *IEEE Trans. Dielectr. Electr. Insul.*, vol. 6, no. 1, pp. 122–130, Feb. 1999.
[16] J. Jiangbo, "Motion of conducting particle near PTFE spacer under AC voltage," *Trans. China Electrotechnical Society*, vol. 23, no. 5, pp. 7–11, May 2008.
[17] J. Wang, Q. Li, B. Li, and C. Chen, "Motion analysis of spherical conducting particle in DC GIL considering the influence of inelastic random collisions and SF6/N2 gaseous mixture," *Proc. CESS*, vol. 35, no. 15, pp. 3971–3978, Aug. 2015.
[18] W. Jian, "Motion and discharge behavior of free conducting wire-type particle within DC GIL," *Proceedigns CSEE*, vol. 36, no. 17, pp. 4793–4801, Sep. 2016.
[19] Y. Khan, "Motion behavior and deactivation method of free-conducting particle around spacer between diverging conducting plates under DC voltage in atmospheric air," *IEEE Trans. Dielectr. Electr. Insul.*, vol. 10, no. 3, pp. 444–457, Jun. 2003.
[20] L. Fangcheng, "Ultrasound characteristics of impact between spherical metal particle and electrode in DC uniform field," *High Voltage App.*, vol. 53, no. 12, pp. 1–7, Dec. 2017.
[21] L. Fangcheng, "Effect of dust in environment-friendly gas on flashover characteristics of epoxy resin," *High Voltage Eng.*, vol. 46, no. 4, pp. 1319–1327, Apr. 2020.
[22] H. Iwabuchi, "Influence of tiny metal particles on charge accumulation phenomena of GIS model spacer in high-pressure SF6 gas," *IEEE Trans. Dielectr. Electr. Insul.*, vol. 20, no. 5, pp. 1895–1901, Oct. 2013.
[23] S. Raghunath Sagar, J. Amarnath, and S. V. L. Narasimham, "Wavelet-based partial discharge signal analysis in GIS," in *Proc. Conf. Electr. Insul. Dielectr. Phenomena*, Vancouver, BC, Canada, 2007, pp. 217–220.
[24] S. Dale and M. Hopkins, "Methods of particle control in SF6 insulated CGIT systems," *IEEE Trans. Power App. Syst.*, vol. PAS-101, no. 6, pp. 1654–1663, Jun. 1982.
[25] A. T. Pérez, "Charge and force on a conducting sphere between two parallel electrodes," *J. Electrostatics*, vol. 56, no. 2, pp. 199–217, Sep. 2002.
[26] M. Hara and M. Akazaki, "A method for prediction of gaseous discharge threshold voltage in the presence of a conducting particle," *J. Electrostatics*, vol. 2, no. 3, pp. 223–237, Jan. 1977.
[27] N. N. LEBEDEV and I. P. SKAL, "Force acting on a conducting sphere in the field of a parallel plane condenser," *Sov. Phys. Tech. Phys.*, vol. 7, pp. 268–270, Jan. 1962.
[28] M. M. Morcos and K. D. Srivastava, "On electrostatic trapping of particle contamination in GITL systems," *IEEE Trans. Power Del.*, vol. 7, no. 4, pp. 1698–1705, Oct. 1992.
[29] B. H. Ma, "Particles and breakdown in SF6- insulated apparatus," *Proc. Inst. Electr. Eng.*, vol. 123, no. 9, pp. 877–881, Sep. 1976.
[30] S. A. F. Matope Van der Merwe and Y. I. Rabinovich, "Silver, copper and aluminium coatings for micro-material handling operations," *South African J. Ind. Eng.*, vol. 24, no. 2, pp. 69–77. Aug. 2013.

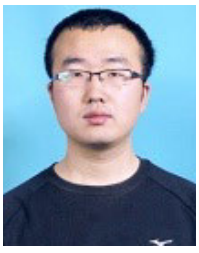

ZHENYU ZHAN received the Ph.D. degree in electrical engineering from North China Electric Power University, Beijing, China, in 2020. He is currently an Engineer with the State Grid Henan Electric Power Research Institute and also a Postdoctoral Fellow with the China Electric Power Research Institute. His main research interests include high voltage, insulation technology, and electrical equipment insulation improvement.

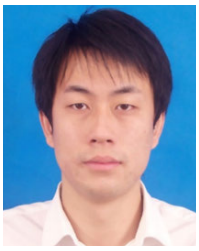

DONG WANG (Member, IEEE) received the Ph.D. degree in high voltage and insulation technology from Wuhan University, Wuhan, China. He is currently a Senior Engineer with the State Grid Henan Electric Power Research Institute. His main research interests include condition evaluation, live line measurement, and defect analysis of primary equipment in substation.

JUN XIE received the Ph.D. degree in electrical engineering from North China Electric Power University, Beijing, China, in 2016. He is currently a Lecturer with North China Electric Power University (Baoding campus). His main research interests include high voltage and insulation technology, and electrical equipment insulation improvement.

WEIFENG XIN received the Ph.D. degree in electrical engineering from Xi'an Jiaotong University, Xi'an, China, in 2015. He is currently a Senior Engineer with the State Grid Henan Electric Power Research Institute. His main research interests include condition evaluation and fault diagnosis of switchgear.

WEI WANG received the B.E. degree in electrical engineering from North China Electric Power University, Baoding, China, in 2001. He is currently a Professor Level Senior Engineer with the State Grid Henan Electric Power Research Institute. His main research interests include high voltage, insulation technology, and electrical equipment insulation improvement.

ZHENQIAN ZHANG received the M.E. degree in electrical engineering from Beijing Jiaotong University, Beijing, China, in 2008. He is currently a Senior Engineer with the China Electric Power Research Institute. His main research interests include condition evaluation and defect analysis of primary equipment in substation.